Charged domain walls under super-band-gap illumination

B. Sturman and E. Podivilov
Institute of Automation and Electrometry, Russian Academy of Sciences, 630090 Novosibirsk, Russia
(Received 14 September 2016; revised manuscript received 27 January 2017; published 10 March 2017)

Charged domain walls (CDWs), which possess metallic-type conductivity and can be created and controlled in the bulk of wide-band-gap ferroelectrics, attract nowadays a strong research interest. The most advanced method for production of stable CDWs involves weak super-band-gap illumination. Here, we investigate theoretically the impact of this illumination on the major wall properties including the energy and the spatial profiles of the polarization, of the electrostatic potential, and of the compensating charge carriers. The key material parameters determining the effect of light are the zero-field polarization strength, the dielectric permittivity, and the trap concentration. The main predictions are substantial reduction of the wall energies and decrease of the electric wall potential under light. These features facilitate creation of dense CDWs patterns and accessibility of the metallic-type wall conductivity.

DOI: 10.1103/PhysRevB.95.104102

I. INTRODUCTION

Charged domain walls (CDWs), which possess metallic-type conductivity and can be created, displaced, and erased in the bulk of nominally nonconducting ferroelectrics, attract nowadays a strong research interest [1–15]. The CDW related highly efficient photovoltaic effects are also at the center of research attention [16–18]. Owing to their unique properties and variability, CDWs are considered as promising elements for the future reconfigurable nanoelectronics [14,19].

Prediction of metallic-type CDW conductivity dates back to the 1970s [20], and it took about 40 years to turn it into reality. Difficulties in creation and control of CDWs in wide-band-gap ferroelectrics are closely related to the necessity of a strong charge compensation of a big bound polarization charge in order to provide the ferroelectric stability [7,20–22]. So far, the most advanced experimental method for production of stable and controllable CDWs patterns involves weak continuous wave (CW) super-band-gap illumination providing the compensating electrons and holes [13]. It is known also that such illumination is sometimes necessary for pronounced CDW conductivity [4].

An appreciable amount of theoretical work (analytical and numerical) has been done on the properties of CDWs (see review [15], papers [20–29], and references therein). This includes analysis of charge screening mechanisms and regimes for different types of walls, determination of the wall widths and energies, mechanism of enhancement of electromechanical response owing to SDWs, investigation of the wall conductivity, the quasiclassical and quantum approaches to the description of the discrete wall energy spectrum. A large necessary amount of the screening charge together with a small CDW width (10–100) nm, result often in huge (for dielectric materials) concentrations of electrons and holes, above $(10^{19}$–$10^{20})$ cm^{-3}. This means the presence of a two-dimensional (2D) sheet of strongly degenerate free carriers possessing metalliclike conductivity.

Remarkably, electrical locality of CDWs, i.e., decay of perturbations of the electric potential far from the wall, was established only recently [29]. This means a pronounced two-scale wall structure with a nanosized *core* incorporating most of the screening charges and pronounced μm-sized *tails*. This general feature affects electrical coupling between individual walls, coupling with electrodes, and also the wall energies. It is due to involvement of localized electronic states in the forbidden gap (which are present in any real crystal) in the charge screening.

The previous studies of the CDW properties dealt with the thermal equilibrium. The latest experimental studies show a surprisingly strong impact of weak super-band-gap illumination on these properties [4,13]. The CDW related photovoltaic properties [16,17] are also detected for super-band-gap illumination. Moreover, the mentioned studies follow the general trend of involvement of light into domain engineering. Thus, the purpose of this paper is to investigate theoretically the impact of super-band-gap illumination on the main CDW characteristics. The band gap of ferroelectric E_g is expected to be much larger than the thermal energy $k_{\mathrm{B}}T$.

The effect of light on the electronic and charge-transport properties is typically described with balance equations for electrons and holes that incorporate the excitation, recombination, and band transport. Appreciable examples of this approach as applied to ferroelectrics, including determination of material parameters, can be found in the studies of the photorefractive phenomena [30,31]. One might expect that application of the balance equations to CDWs is especially complicated because of a strong spatial nonuniformity, degeneration of charge carriers, and involvement of the ferroelectric degrees of freedom. It turns out, however, that the mentioned specific properties of CDWs enables one to strongly simplify the treatment of the effect of light.

The positively and negatively charged CDWs are overwhelmingly compensated by electrons and holes, respectively, i.e., the charge screening is almost monopolar for each individual wall. Since the lifetimes of photoexcited electrons and holes are typically much longer than the thermalization times, dependences of their concentrations n and p on the electric potential φ can still be described by the relations of the Fermi statistics as applied to semiconductor band models. The main difference between the thermal and light-induced dependences $n(\varphi)$ and $p(\varphi)$ is that instead of the Fermi energy F we must use certain intensity-dependent quasi-Fermi energies $F_{n,p}$ [32,33]. Employment of the quasi-Fermi-energy approach makes our theory simple and compact. It enables us

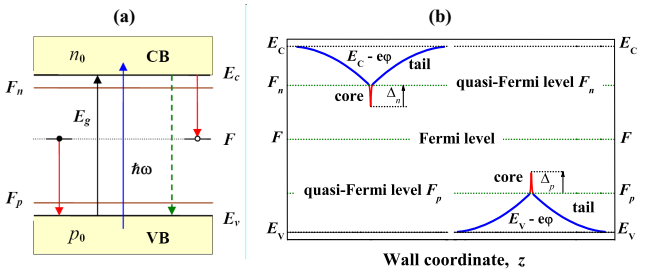

FIG. 1. (a) Energy scheme and light-induced transitions for spatially uniform ferroelectric. Super-band-gap illumination produces electron-hole pairs, and recombination occurs mostly via localized levels in the forbidden gap. (b) Schematic of the spatial structure of positive (left) and negative (right) CDWs. Electrons and holes are degenerate in the cores and nondegenerate in the tails. The energy distances are exaggerated and the core drops Δ_n and Δ_p are generally different.

to describe most of the CDW properties. Nevertheless, we use the balance equations to justify additionally this approach and consider some important issues lying beyond it.

II. THEORETICAL BACKGROUND

The principal energy scheme of a spatially uniform ferroelectric is depicted in Fig. 1(a). Continuous-wave (CW) illumination with the light-quantum energy $\hbar\omega$ exceeding the band gap E_g excites electrons and holes in the conduction band (CB) and in the valence band (VB). Recombination of electrons and holes occurs via partially filled traps at the Fermi level F. While this linear recombination is expected to be dominating for low intensities, the quadratic electron-hole recombination is also allowed. The spatially uniform concentrations of electrons and holes are n_0 and p_0. The quasi-Fermi levels F_n and F_p lie between the Fermi level and the edges of conduction and valence bands E_c and E_v, respectively (see also below).

Figure 1(b) announces the energy structure of CDWs for the charge screening by degenerate electrons and holes; z is the across-wall coordinate. The electrostatic wall potential $\varphi(z)$ shifts the cores below and above the quasi-Fermi levels F_n and F_p for positive and negative CDWs, respectively. Far enough from the walls we return to the spatially uniform case.

The positive (head-to-head) CDWs can be of 180° ($\rightarrow|\leftarrow$) or 90° ($\nearrow|\nwarrow$) type. The same is valid for the negative (tail-to-tail) CDWs where the direction of spontaneous polarization $\mathbf{P}_0$ is inverted. In any case, the problem is one dimensional: all variables depend on a single wall coordinate z. The basic case for us is the 180° walls; the results for the 90° walls can be obtained by a simple renormalization procedure [28].

The basic relations for the spontaneous polarization $P_z = P$ and the electrostatic potential φ are not different from those used and justified in [22,29]:

$$-\frac{d\varphi}{dz} = \alpha P + \beta P^3; \quad \frac{dP}{dz} = \rho, \tag{1}$$

where $\alpha < 0$ and $\beta > 0$ are constants and $\rho = \rho(z)$ is the compensating free charge density. The first relation is the equation of state for the ferroelectric second-order transition. The combinations $\varepsilon = 2\pi/|\alpha|$ and $P_0 = \sqrt{|\alpha|/\beta}$ give the main contribution to the dielectric constant of the ferroelectric and the zero-field spontaneous polarization, respectively. Omission of the correlation term ($\propto \partial^2 P/\partial z^2$) in the first relation is justified for CDWs, where the strong charge compensation mechanism prevents formation of large gradients. The second relation comes from Maxwell's electrostatic equation $dD/dz = 4\pi\rho$ taking into account that ε strongly exceeds the background contribution to the dielectric constant.

Typically, the charge density ρ can be treated as a function of φ [22,29]. In this most common case, P can also be considered as a function of φ, and Eqs. (1) give after an elementary integration the following important integral relation:

$$\frac{\pi P_0^2}{2\varepsilon}\left(1 - \frac{P^2}{P_0^2}\right)^2 + \int_0^{\varphi} \rho(\varphi')\, d\varphi' = 0. \tag{2}$$

It accounts for the fact that $P(z) \to \pm P_0$ and $\varphi(z) \to 0$ for the distance to the wall center $|z| \to \infty$. Furthermore, it allows to express algebraically P by φ for any particular model of $\rho(\varphi)$ and deal further only with the first-order differential equation (1) for φ.

The key issue of CDW modeling is the dependence $\rho(\varphi)$, which incorporates a great deal of information about population of delocalized and localized energy levels. In the case of thermal equilibrium, the relations of the Fermi statistics for electrons and holes strongly simplify the matter [22,29]. However, they are invalid in the case super-band-gap illumination. The most common approach here is employment of a set of balance equations for electrons and holes incorporating the light-induced transitions, the recombination processes, and the charge transport [30,31]. These equations are model specific, cumbersome, and difficult for analytical and numerical treatments. At the first sight, investigations of CDW properties under light have to be especially difficult because of a strong spatial nonuniformity and a large amount of screening charge. However, just these features allow us to strongly simplify the treatment.

It is clear that screening of positive and negative CDWs is predominantly accomplished by electrons and holes, respectively. For positive CDWs, the concentration of free electrons n is much larger than the concentration of holes p and the steady-state electronic current density j_n is zero in the leading approximation. Similarly, we have $p \gg n$ and $j_p \simeq 0$ for negative CDWs. Next, we take into account that the lifetimes of photoexcited charge carriers are typically much longer than their thermalization times. Altogether, this means that the dependence $n(\varphi)$ for positive CDWs and the dependence $p(\varphi)$ for negative CDWs obey the relations of Fermi statistics with only one exception: the Fermi energy F has to be replaced by the quasi-Fermi energies F_n and F_p which are different from F and from each other [32,33]. These energies depend generally on the light intensity and on distribution of localized energy levels in the forbidden gap.

Employing the standard parabolic CB model, we have for the concentration of electrons in this band [32]

$$n = N_n \Phi\left(\frac{F_n - E_c + e\varphi}{k_B T}\right), \tag{3}$$

where e is the elementary charge, $N_n = 2(m_n k_B T/2\pi\hbar^2)^{3/2}$ is the effective CB density of states, m_n is the effective electron mass, T is the temperature, k_B is the Boltzmann constant, and

$$\Phi(\zeta) = \frac{2}{\sqrt{\pi}} \int_0^\infty \frac{x^{1/2}\, dx}{1 + \exp(x - \zeta)} \tag{4}$$

is the Fermi-Dirac integral of index $\frac{1}{2}$. At $T = 300$ K and for m_n equal to the naked electron mass m_0, we have $N_c \simeq 2.5 \times 10^{19}$ cm^{-3}. Furthermore, we have $\Phi(\zeta) \simeq \exp(\zeta)$ for $\zeta \leqslant -1$; this is the case of *nondegenerate* Boltzmann electrons with the concentration $n \ll N_n$. In the opposite case $\zeta \geqslant 2$, we have $\Phi \simeq 0.75\,\zeta^{3/2}$. This is the case of *degenerate* electrons with the T-independent Thomas-Fermi concentration $n(\varphi) \simeq 0.1 m_n^{3/2}\hbar^{-3}\,(F_n - E_c + e\varphi)^{3/2} \gg N_n$. Analogous relations are valid for the hole concentration $p(\varphi)$. They include the effective VB density of states N_p, the effective hole mass m_p, and the quasi-Fermi energy F_p.

Far enough from CDWs, when the potential $\varphi(z)$ is already close to zero, the electron or hole concentrations tend to spatially uniform values n_0 and p_0. The same values correspond to a uniform illumination of a single-domain ferroelectric and manifest themselves, e.g., in photoconductivity. For continuous-wave light intensity I, we have safely $n_0(I), p_0(I) \lll N_{n,p}$. The charge carriers in this range are strongly nondegenerate. The quasi-Fermi energies can thus be expressed by small intensity-dependent ratios $r_n = n_0/N_n$ and $r_p = p_0/N_p$:

$$F_{n,p} = E_{c,v} \pm k_B T \ln r_{n,p}(I). \tag{5}$$

With increasing light intensity I, F_n and F_p shift gradually towards E_c and E_v, respectively. It is worthy of mentioning that the uniform concentrations n_0 and p_0 are just an equivalent of the quasi-Fermi energies E_n and E_p. While the link (5) is quite general, the functions $n_0(I)$ and $p_0(I)$ are model dependent: they must include different ionization and recombination constants. With increasing I, the linear recombination to the traps transforms usually into quadratic electron-hole recombination. Up to Sec. VI, where we consider the simplest semiconductor model, the concentrations n_0 and p_0 are treated as independent physical quantities.

In wide-band-gap materials, the light-induced concentrations n_0 and p_0 are typically many orders of magnitude larger than the thermal concentrations n_T and p_T. This means that F_n and F_p lie well above and below the Fermi level F. Only for extremely small intensities, when $n_0, p_0 \to n_T, p_T$, the quasi-Fermi levels $F_{n,p}$ approach F.

Not only CB electrons and VB holes participate in the CDW screening. The so-called trap recharging, i.e., spatial modulation of the electrons on localized energy levels in the forbidden gap, is also involved. In particular, the trap recharging is responsible for the CDW tails in thermal equilibrium and contributes to the wall energies [29]. Let the total trap concentration be $N_t = \text{const}$, while the concentrations of filled and empty traps be $N_\bullet = N_\bullet(z)$ and $N_\circ = N_\circ(z)$, so that $N_\bullet + N_\circ = N_t$. The spatially uniform thermal values of $N_{\bullet,\circ}$ are $N^T_{\bullet,\circ}$. Taking into account neutrality of ferroelectric in thermal equilibrium far from the wall, we see that the contributions of the localized electrons and holes to the charge density are $-e(N^T_\circ - N_\circ)$ and $e(N^T_\bullet - N_\bullet)$, respectively.

As soon as $n \gg p$ near the positive CDWs, the electron recombination to empty traps cannot be compensated by the hole recombination. This means a strong trap saturation, i.e., the equality $N_\circ \simeq 0$ for the scheme of Fig. 1(a). Similarly, near the negative CDWs we have $p \gg n$ and $N_\bullet \simeq 0$. The total charge density ρ near the positive and negative CDWs is thus given by the relations

$$\rho = -e(N^T_\circ + n) \quad \text{and} \quad \rho = e(N^T_\bullet + p), \tag{6}$$

respectively. The concentrations $N^T_{\bullet,\circ}$ have to be treated as material characteristics. They are also relevant to various photoelectric and photorefractive phenomena and can be estimated from experiments [30,31].

The above relations are sufficient to determine most of the CDW characteristics. However, they are insufficient to quantify the contributions of minor charge carriers and the transition to no trap saturation far from the walls. To fill this gap and to justify additionally employment of the quasi-Fermi-level approach, balance equations for electrons and holes are needed. They are presented and analyzed in Sec. VI.

While our theory provides dependences of the CDW characteristics on the key intensity-independent parameters $P_0, \varepsilon, N_{n,p}$, and $N^T_{\bullet,\circ}$, representative values of these parameters are useful for numerical estimates. For this purpose, we use $P_0 = 30\,\mu$C/cm^2, $\varepsilon = 500$, $N_{n,p} = 10^{19}$ cm^{-3}, and $N^T_{\bullet,\circ} = 10^{17}$ cm^{-3}. The values of P_0 and ε are representative for perovskites. The values of $N_{n,p}$ correspond to the mass ratio $m_{n,p}/m_0 \simeq 0.5$; they account for the fact that the effective masses of electrons and holes are often smaller in semiconductors as compared to m_0. The representative values of $N^T_{\bullet,\circ}$ lie in the middle of the range (10^{16}–10^{18}) cm^{-3} typical for trap concentrations in undoped ferroelectrics [30].

The variation range of the intensity-dependent ratios $r_n(I) = n_0/N_n$ and $r_p(I) = p_0/N_p$ is generally huge. From below, they are restricted to n_T/N_n and p_T/N_p. For the forbidden gap $E_g = 3$ eV and the Fermi energy F lying in the middle of this gap, we have $n_T/N_n \sim p_T/N_p \sim 10^{-25}$. From above, the expected restriction is $r_{n,p} \ll N^T_{\bullet,\circ}/N_{n,p} \approx 10^{-2}$. It corresponds to the absence of trap saturation for single-domain samples. For illustrations, we choose the range $10^{-7} \leqslant r_{n,p} \leqslant 10^{-3}$ as representative (see also the estimates of Sec. VI).

III. WALL-CENTER CHARACTERISTICS

Let us consider for definiteness the case of positive CDWs. It is evident that the polarization $P(z)$ turns to zero at the wall center $z = 0$, while the potential $\varphi(z)$ and the electron concentration $n(z)$ reach here their maxima. Setting $P = 0$ in Eq. (2) and using Eqs. (3)–(6), we obtain for the maximum value of $u = e\varphi/k_B T$

$$(N^T_\circ/N_n)\, u + \tilde{\Phi}(u, r_n) = \kappa_n \equiv \pi P_0^2/2\varepsilon k_B T N_n, \tag{7}$$

where κ_n is the characteristic parameter including only intensity-independent quantities and

$$\tilde{\Phi}(u, r_n) = \frac{2}{\sqrt{\pi}} \int_0^\infty x^{1/2} \ln\left(\frac{e^x + r_n e^u}{e^x + r_n}\right) dx \tag{8}$$

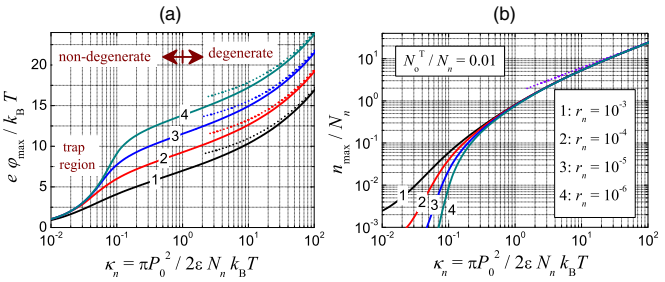

FIG. 2. Dependence of $u_{\max} = e\varphi_{\max}/k_BT$ (a) and $n_{\max}/N_n$ (b) on κ_n for $N_\circ/N_n = 0.01$ and four values of the intensity-dependent ratio $r_n = n_0(I)/N_n$. The dotted lines correspond to the asymptotic relations for strongly degenerate electrons.

is a new Fermi integral. Equation (7) expresses the competition between the CB and trapped electrons in the CDW screening. For sufficiently small (large) values of κ_n, the first (second) term in its left-hand side is dominating. As the function $u_{\max}(\kappa_n)$ is known, the dependence $n_{\max}(\kappa_n)$ can be determined from Eqs. (3) and (5). Generalization to the case of negative CDWs is evident.

Figure 2 gives an overview of the situation. The solid lines in Figs. 2(a) and 2(b) show $u_{\max}$ and $n_{\max}/N_n$ versus κ_n for $N_\circ^T/N_n = 0.01$ and four representative values of the intensity-dependent parameter r_n on semilogarithmic and double-logarithmic scales. Several distinctive features are clearly seen:

(i) The regions $\kappa_n \gg 1$ and $\kappa_n \ll 1$ correspond to strongly degenerate and strongly nondegenerate CB electrons, respectively, the values $\kappa_n \sim 1$ are intermediate. This can also be deduced from Eq. (7). Thus, we have got a simple and general criterion of degeneracy; it is important also for thermal equilibrium.

(ii) For $\kappa_n \lesssim 0.1$, we have the trap screening region. Here, $u_{\max}$ weakly depends on $r_n = r_n(I)$, while the r_n dependence of $n_{\max}/N_n$ is strongly pronounced. This feature is qualitatively clear: Since the trapped electrons are sufficient for screening, the CB electrons are of minor importance.

(iii) Outside the trap region, when $\kappa_n \gg 0.1$, $u_{\max}$ grows steadily with decreasing $r_n(I)$, while $n_{\max}/N_n$ stays practically constant in r_n.

(iv) For $\kappa_n \gg 1$, the solid lines approach the corresponding dotted lines expressing the asymptotic properties of the strongly degenerate electron system.

Two last features require an additional clarification. They are relevant to the asymptotic properties of the Fermi integrals Φ and $\tilde{\Phi}$. Using Eqs. (4), (7), and (8), one can find that $u_{\max} \simeq \ln(\kappa_n/r_n)$ and $n_{\max} \simeq N_n\kappa_n$ for strongly nondegenerate electrons outside the trap region. These asymptotic relations reproduce the above mentioned features of Fig. 2. However, the field of their applicability, $0.1 \ll \kappa_n \ll 1$, is narrow for the chosen ratio $N_\circ^T/N_n = 10^{-2}$. For strongly degenerate electrons $\kappa_n \gg 1$, one can find the following asymptotic relations: $u_{\max} = -\ln r_n(I) + (15\sqrt{\pi}\kappa_n/8)^{2/5}$, $n_{\max}/N_n = (15\sqrt{\pi}\kappa_n/8)^{3/5}$. They give an r_n-dependent value of $u_{\max}$ and an r_n-independent value of $n_{\max}/N_n$ and are shown by the dotted lines in Fig. 2.

Furthermore, it is not difficult to find using the definitions of κ_n and N_n that the above asymptotic relations can be rewritten as

$$F_n - e\varphi_{\max} = \Delta_n \simeq 4.35 \times \left(P_0^4\hbar^6/\varepsilon^2 m_n^3\right)^{1/5},$$
$$n_{\max} \simeq 1.18 \times \left(m_n^3 P_0^6/\varepsilon^3\hbar^6\right)^{1/5}. \quad (9)$$

The values of Δ_n and $n_{\max}$ depend neither on the intensity-dependent parameter r_n nor on the temperature T. They are not different from the core energy drop and the maximum electron concentration in the thermal equilibrium, respectively [see also Fig. 1(b)]. The effect of light is present only in the first contribution to $e\varphi_{\max}$. This suggests that the presence of light reduces merely the energy distance to the core $E_c - F_n = -k_BT \ln r_n$ compared to the thermal distance $E_c - F$. Relations (9) correspond to the quasiclassical Thomas-Fermi approximation for degenerate electrons.

Now, we make some numerical estimates using the representative values of P_0, N_n, and ε indicated in the end of Sec. II. For the characteristic parameter κ_n we obtain at room temperature $\kappa_n \simeq 60$. This corresponds indeed to strongly degenerate electrons. The case of nondegenerated electrons $\kappa_n \lesssim 1$ cannot be excluded, but it seems to be less common and interesting. Next, we get for the core drop $\Delta_n \simeq 0.2$ eV. This is smaller than or comparable with the distance to the core $E_c - F_n = k_BT \ln(1/r_n)$. In particular, when $r_n = n_0/N_n$ ranges from 10^{-7} to 10^{-3}, this energy distance changes from $\simeq$0.4 to 0.2 eV. In turn, this distance is substantially smaller than its thermal value $E_c - F = k_BT \ln(N_n/n_T)$.

IV. CDW PROFILES

To find the spatial profile $u(z) = e\varphi(z)/k_BT$ for a positive CDW, we employ the second of Eqs. (1), set $P = P(u)$, and express the derivative dP/du by u from Eq. (2). Next, using Eqs. (3) and (6) for $\rho(n)$ and $n(u)$, we arrive at an ordinary first-order differential equation for $u(z)$; it can be integrated numerically. With the profile $u(z)$ known, we calculate algebraically $n(z)$ and $P(z)$ from Eqs. (2) and (3), respectively.

Some characteristic spatial scale has to be chosen for normalization of the wall coordinate z. This choice is not unique because of the simultaneous presence of different spatial ranges of CDW screening relevant to the degenerate, nondegenerate, and trapped electrons. Our primary choice is the Debye screening radius

$$R_D = (\varepsilon k_BT/4\pi N_n e^2)^{1/2} \quad (10)$$

relevant to the CB density of states N_n. This scale is intermediate between the Thomas-Fermi screening length $R_{TF} = (\varepsilon^3\hbar^6/P_0 m_n^3 e^5)^{1/5}$ corresponding to strongly degenerate electrons [29] and the Debye screening length $\tilde{R}_D = (\varepsilon k_BT/4\pi N_\circ^T e^2)^{1/2} = R_D\sqrt{N_n/N_\circ^T}$ relevant to trapped electrons. For the above chosen representative parameters we have $R_D \simeq 8.5$ nm, $R_{TF} \simeq 6$ nm, and $\tilde{R}_D \simeq 85$ nm.

Figure 3 shows representative spatial profiles of $u = e\varphi/k_BT$, n/N_n and P/P_0 for positive CDWs. The left panel [Figs. 3(a)–3(c)] corresponds to the characteristic parameter $\kappa_n = 60$, while the right panel [Figs. 3(d)–3(f)] corresponds to $\kappa_n = 0.6$. Only two representative values of the intensity-

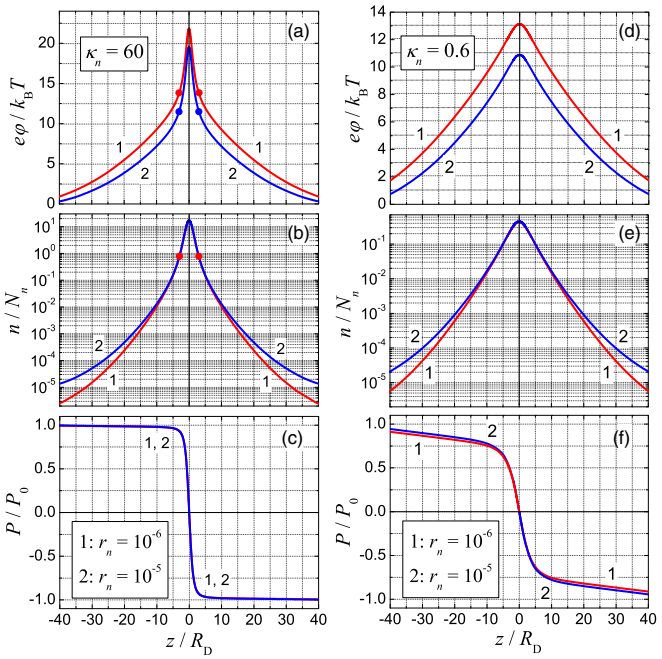

FIG. 3. Positive CDWs: spatial profiles of $u = e\varphi/k_BT$, n/N_n, and P/P_0 for $\kappa_n = 60$ [(a)–(c)] and for $\kappa_n = 0.6$ [(d)–(f)]. Lines 1 and 2 correspond to $r_n = 10^{-6}$ and 10^{-5}, respectively. The filled circles in (a) and (b) indicate the borders between the regions of degenerate and nondegenerate electrons.

dependent ratio $r_n = n_0(I)/N_n$ are considered; this is sufficient to illustrate the main features.

The presence of a short-range core and a long-range tail is clearly seen for each profile $u(z)$ in Fig. 3(a). The core is due to degenerate electrons; the filled circles on each line indicate the borders between the regions of degenerate and nondegenerate electrons where $n(z) = N_c$. The values of $u(0) = u_{\max}$ correspond to Eq. (7) and to the relevant points on Fig. 2(a). Decreasing ratio r_n leads mostly to a vertical rise of the curves $u(z)$. Within the tails, the CDW screening by nondegenerate CB electrons transfers smoothly to the screening by the trapped electrons. The tails are obviously much longer than R_D.

The curves in Fig. 3(b) would be undistinguishable on a linear vertical scale. The logarithmical scale used shows the difference in the curves for $r_n = 10^{-6}$ and 10^{-5} on the far tails corresponding to the trap regions. The polarization profiles are also undistinguishable on the linear scale [see Fig. 3(c)]. They show practically no long-range features. The width of the polarization profile, calculated between the points where $P(z) = \pm P_0/2$, is $w \simeq 1.46R_D \simeq 2R_{\rm TF}$.

The CDW profiles of the right panel of Fig. 3, corresponding to $\kappa_n = 0.6$, show not only similarities with with the profiles of the left panel, but also new features. Breaking the profile $u(z)$ down to core and tails is practically absent in Fig. 3(d), and the width of this profile is much larger than R_D. The trap region is more pronounced in Fig. 3(e) compared to Fig. 3(b). Convergence of $P(z)$ to the limiting values $\pm P_0$ with increasing $|z|$ occurs relatively slow, especially for $|z|/R_D \gg 1$. The smaller $r_n(I)$, the slower is this convergence. The width of the polarization profiles is here about $6R_D$.

The tail length ℓ for Fig. 3(a) admits a simple analytical estimate. To make it, we indicate that most of the potential drop for the tail occurs in the trap region where $u(z) \lesssim \ln(N_\circ^T/r_nN_n)$, $\rho \simeq -eN_\circ^T$, and P is already close to $\pm P_0$. Thus, we have a parabolic potential profile, which turns to zero at $|z| \simeq \ell$, where

$$\ell = R_D\sqrt{2\,\ln(N_\circ^T/r_nN_n)\,N_n/N_\circ^T}. \tag{11}$$

This relation gives a weak logarithmical increase of ℓ with decreasing $r_n(I)$. For $N_\circ^T/N_n = 10^{-2}$ and $r_n = 10^{-6}$, we have $\ell \simeq 43R_D \simeq 0.36\ \mu$m in a good agreement with Fig. 3(a). This value gives also a rough estimate of the half-width of the polarization profile for $\kappa_n \lesssim 1$ [see Fig. 3(d)].

The results on the behavior of p/n and $N_\bullet/N_t$ far from the wall can be found in Sec. VI. They are obtained with the balance equations for electrons and holes.

V. EFFECT OF LIGHT ON WALL ENERGIES

An important consequence of the above analysis is that super-band-gap illumination leads to a substantial *lowering of the wall energies* as compared to their thermal values. The CDW energy W (per a unit surface element) is the difference between the energies of ferroelectric with and without the wall. It is positive and given by $W = -\int \rho(z)\varphi(z)\,dz$ [29]. In the most common case of degenerate electrons, the compensating charge is localized mostly at the core where $e\varphi \simeq E_c - F_n$. In this case, the energy of the positive wall can be estimated as

$$W_n \simeq \frac{2P_0}{e} \times [0.7\Delta_n + k_BT\,\ln(N_n/n_0)]. \tag{12}$$

The first term in the square brackets accounts for the structure of the core, where both $\rho(z)$ and $\varphi(z)$ vary quickly [29]; this term is typically relatively small. An analogous estimate, with the replacements $N_n \to N_p$ and $\Delta_n \to \Delta_p$, is valid for the negative wall energy W_p.

To get the thermal wall energies W_n^T and W_p^T, it is sufficient to replace $k_BT\,\ln(N_n/n_0)$ and $k_BT\,\ln(N_p/p_0)$ in the expressions for W_n and W_p by $E_c - F$ and $F - E_v$, respectively. This leads to the known estimate of the total thermal energy $W_n^T + W_p^T \simeq (2P_0/e) \times E_g$ [11,22].

In the case of nondegenerate electrons, $\kappa_n \ll 1$, the core is not pronounced, but the the electron concentration and the charge density still possess sharp peaks at $z = 0$. The wall energies can be estimated here as

$$W_{n,p} \simeq \frac{2P_0}{e} \times k_BT\,\ln\left(\frac{\kappa_{n,p}}{r_{n,p}}\right). \tag{13}$$

They are slightly smaller compared to values of $W_{n,p}$ relevant to the degenerate case.

Let us now estimate the ratio of the total wall energies under illumination and in the thermal equilibrium. Regardless of the degeneration degree, it is given by

$$\frac{W}{W_T} = \frac{W_n + W_p}{W_n^T + W_p^T} \simeq \frac{k_BT}{E_g}\,\ln\left(\frac{N_nN_p}{n_0p_0}\right). \tag{14}$$

The larger the light intensity, the smaller is the energy ratio. In the opposite limit, $n_0 \to n_T$ and $p_0 \to p_T$, it tends to 1. For $n_0 \gg n_T$ and $p_0 \gg p_T$, the ratio W/W_T can be substantially

smaller than 1. In particular, setting $N_n/n_0 = N_p/p_0 = 10^3$ and $E_g = 3$ eV, we obtain $W/W_T \simeq 0.1$.

VI. LINK TO BALANCE EQUATIONS

The purpose of this section is twofold:

(i) First, we intend to formulate a set of balance equations for the concentrations n, p, and $N_\bullet$ incorporating the main ingredients of CDW screening. Generally speaking, balance equations of this kind are known, especially in the area of photorefraction [30,31,34]. However, our case is very special owing to large attracting potentials and strong degeneration of the major charge carriers near the walls. The well-known Einstein relations between the diffusion coefficients and mobilities of the carriers are invalid here. Employment of these relations for CDW screening modeling, like it was done in [3,7], leads to Boltzmann statistics instead of Fermi one and to noncontrollable errors. To the best of our knowledge, the necessary balance equations for CDW screening were never formulated.

(ii) Second, we are going to employ the balance equations to express the former uniform concentrations n_0 and p_0 by the light intensity I, to justify additionally the quasi-Fermi-energy approach, and to demonstrate the possibility to proceed beyond the range of applicability of this approach. The latter concerns far periphery of CDWs where the minor charge carriers become non-negligible and the traps become nonsaturated.

A. General properties

The scheme of Fig. 1(a) corresponds to the following set of balance equations for the electron and hole concentrations n and p and the filled trap concentration $N_\bullet$:

$$\frac{\partial n}{\partial t} - \frac{1}{e}\frac{\partial j_n}{\partial z} = g - \gamma_n n N_\circ - \gamma n p,$$
$$\frac{\partial p}{\partial t} + \frac{1}{e}\frac{\partial j_p}{\partial z} = g - \gamma_p p N_\bullet - \gamma n p,$$
$$\frac{\partial N_\bullet}{\partial t} = \gamma_n n N_\circ - \gamma_p p N_\bullet. \qquad (15)$$

Here, $\gamma_{n,p}$ and γ are recombination constants characterizing the linear and quadratic recombination, g is the rate of light-induced transitions, $N_\bullet + N_\circ = N_t$,

$$j_n = e\mu_n n\mathcal{E} + eD_n\frac{\partial n}{\partial z} \quad \text{and} \quad j_p = e\mu_p p\mathcal{E} - eD_p\frac{\partial p}{\partial z} \qquad (16)$$

are the electron and hole current densities, $\mu_{n,p}$ and $D_{n,p}$ are the corresponding mobilities and diffusion coefficients, and $\mathcal{E} = -\partial\varphi/\partial z$ is the electric field. Thermal excitation is neglected for simplicity, so that the concentrations $N^T_{\bullet,\circ}$ can be identified with the dark concentrations, and the total charge density is $\rho = -e(n - p + N_\bullet - N^T_\bullet)$. The excitation rate g can be expressed by the light absorption coefficient $\alpha_{\rm abs}$ and the light intensity I: $g = \alpha_{\rm abs} I/\hbar\omega$.

For sufficiently low intensities, when the linear recombination is dominating over the quadratic one, the uniform concentrations of electrons and holes are $n_0 = g\tau_n$ and $p_0 = g\tau_p$, where $\tau_n = 1/\gamma_n N^T_\circ$ and $\tau_p = 1/\gamma_p N^T_\bullet$ are the characteristic lifetimes. This linear regime occurs for $\gamma g\,\tau_n\tau_p \lesssim 1$. In the opposite case, the linear growth of $n_0(g)$ and $p_0(g)$ changes to a square-root one $n_0 \simeq p_0 \simeq \sqrt{g/\gamma}$. Changeover to the square-root dependence occurs usually in the mW/cm^2 intensity range and sharply depends on $\hbar\omega$ [31,34]. Let us estimate the uniform concentrations for the linear excitation regime. Setting $\alpha_{\rm abs} \sim 100$ cm^{-1}, $I \sim 10$ mW/cm^2, $\tau_{n,p} \sim 1$ ns, and $\hbar\omega \approx 3$ eV, we obtain $n_0, p_0 \sim 10^{10}$ cm^{-3}. This rough estimate shows that the inequalities $n_0, p_0 \ll N_\bullet, N_\circ$ are safely fulfilled.

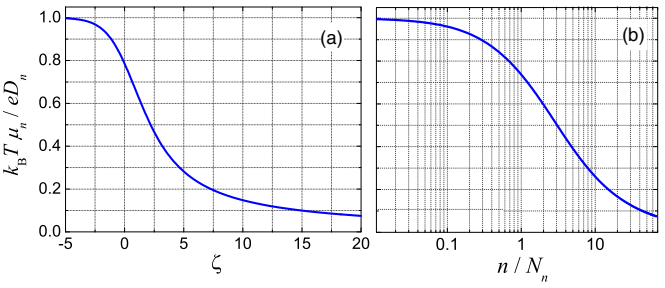

FIG. 4. Generalization of the Einstein relation for electrons: the ratio $k_{\rm B}T\mu_n/eD_n$ versus ζ (a) and the ratio n/N_n (b).

While the structure of Eqs. (16) for $j_{n,p}$ is the same for degenerate and nondegenerate carriers, the ratios $D_{n,p}/\mu_{n,p}$ cannot generally be treated as constants in φ. Constancy of these ratios occurs only for nondegenerate carriers. In this very case, the known Einstein relation $D_{n,p}/\mu_{n,p} = k_{\rm B}T/e$ holds true, and the conditions $j_{n,p} = 0$ (which must be fulfilled in thermal equilibrium) give Boltzmann's dependences $n(\varphi)$ and $p(\varphi)$. Furthermore, it is clear that the ratios $D_{n,p}/\mu_{n,p}$ must grow with increasing degeneration degree because diffusion towards lower concentrations (and areas with weaker degeneration) is profitable.

Generalization of the Einstein relations for degenerate charge carriers is known in the semiconductor physics [33,35,36]. It reads as for electrons

$$k_{\rm B}T\mu_n/eD_n = d\,\ln\Phi(\zeta)/d\zeta, \qquad (17)$$

where $\zeta = (F_n - E_c + e\varphi)/k_{\rm B}T$, $\Phi(\zeta)$ is given by Eq. (4), and $F_n \to F$ in thermal equilibrium. For $\zeta \ll -1$ we return to the Einstein relation. Since $n/N_n = \Phi(\zeta)$ according to Eq. (3), the ratio $\mu_n k_{\rm B}T/eD_n$ can also be considered as a function of n/N_n.

Figures 4(a) and 4(b) show this ratio versus ζ and n/N_n. As expected, the ratio D_n/μ_n grows with increasing ζ and n/N_n. The effect of degeneration can be very strong.

Since Eq. (17) is derived from the condition of zero electronic current in thermal equilibrium [33,35,36], it is evident that any approximations for the balance equations leading to dominating current j_n (or j_p) correspond to the results of Secs. II–V. The arguments for such approximations are simple: in steady state, the total current density $j_n + j_p$ is zero. Photoexcited electrons (holes) are attracting to (repulsing from) a positive CDW. As soon as the wall potential is large, $e\varphi_{\max} > (2-3)k_{\rm B}T$, one can expect that $n \gg p$ and $|j_n| \gg |j_p|$ not far enough from the wall center. The remaining questions are about the application area of

such approximations and the possibility to describe the CDW structure beyond this area.

B. Particular results

We consider only the steady-state situation, i.e., set $\partial/\partial t = 0$ in Eqs. (15). To avoid cumbersome expressions, we make a number of secondary simplifications: we consider the fully symmetric case $\gamma_{n,p} = \gamma$, $D_{n,p} = D$, $N_\bullet^T = N_\circ^T = N_t/2$, $\tau_{n,p} = \tau$, and $p_0 = n_0$. Furthermore, we neglect the quadratic recombination and focus on the case of nondegenerate charge carriers $\kappa_{n,p} \lesssim 1$. The last assumption is not obligative because electrons are always nondegenerate far from the wall.

With these simplifications, we express first the ratio p/n by $N_\bullet$ from the third of Eqs. (15):

$$p/n = N_t/N_\bullet - 1. \tag{18}$$

This gives $N_\bullet \simeq N_t$ for $p/n \ll 1$ and $N_\circ \simeq N_t$ for $n/p \ll 1$. Just these cases occur near the positive and negative CDWs. Second, we obtain for $u = e\varphi/k_B T$ from the equality $j_n + j_p = 0$ using Eqs. (16):

$$u_z = (n-p)_z/(n+p), \tag{19}$$

where the subscript z indicates the spatial differentiation. Third, excluding $N_\circ$ and φ_z from the first of Eqs. (15) with the help of Eqs. (18) and (19), we get

$$\frac{np}{n+p} - L_D^2\left[\frac{(np)_z}{n+p}\right]_z = \frac{n_0}{2}, \tag{20}$$

where $L_D = (D\tau)^{1/2}$ is the diffusion length. The second term in Eq. (20) is small as compared to the first one when the characteristic scale in z, which is expected to be $\tilde{R}_D = (\varepsilon k_B T/4\pi N_\bullet^T e^2)^{1/2}$, is substantially larger than L_D. This special physical condition is typically well fulfilled (see also below). Neglecting the second term in Eq. (20) and using Eqs. (18) and (19), we obtain after simple calculations

$$u = 1 - 2y + \ln\left(\frac{y}{1-y}\right), \tag{21}$$

$$\rho = \frac{e(1-2y)}{2}\left[N_t + \frac{n_0}{y(1-y)}\right], \tag{22}$$

where $y = N_\bullet/N_t$ is the trap saturation parameter ranging from 0 to 1. These relations are valid for both positive and negative CDWs regardless of the values of n/p and $N_\bullet/N_t$. They satisfy all necessary physical requirements. In particular, $u = 0$ for $y = \frac{1}{2}$ and tends to $\pm\infty$ for $y \to 1$ and 0.

Using Eqs. (21) and (22), we can calculate analytically the integral $\int_0^\varphi \rho(\varphi')d\varphi'$ entering Eq. (2). After that, employing Eqs. (1) one can find numerically the z dependences of u, n/N_n, P/P_0, n/p, and $N_\bullet/N_t$ for any $r_n = n_0/N_n$. For $\kappa_n = 0.6$, $r_n = 10^{-5}$ and 10^{-6}, and $|z|/R_D \lesssim 40$, the first three dependences nicely reproduce those given in the right panel of Fig. 3. In the far-tail region, $|z|/R_D \gtrsim 40$, they tend monotonically (without special features) to 0, n_0/N_n, and ∓ 1, respectively. This proves validity of the above treatments of the balance equations and extends the limits of our theory to far tails. The last two dependences, which demonstrate transition to nonperturbed values of n/p and $N_\bullet$ far from the wall and cannot be obtained within the quasi-Fermi-level approach, are present in Fig. 5.

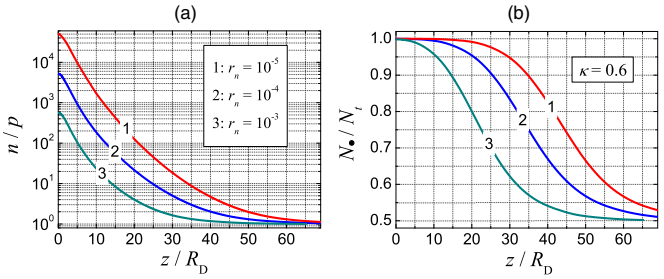

FIG. 5. Spatial profiles of n/p (a) and $N_\bullet/N_t$ (b) for three values of $r_n = n_0/N_n$ obtained with Eqs. (21) and (22) for a positive CDW with $\kappa_n = 0.6$.

One sees that $n \gg p$ and $N_\bullet \simeq N_t$ not far from the wall center where $u \gtrsim 1$. However, far enough from the wall, when $u \lesssim 1$, these relations become invalid. In particular, for $r_n = n_0/N_n = 10^{-5}$ they hold true for $z/R_D \lesssim 40$, which is consistent with the right panel of Fig. 3. For larger distances from the wall, the ratios n/p and $N_\bullet/N_t$ tend exponentially to 1 and $\frac{1}{2}$, respectively. The smaller r_n, the slower is the transition to the limiting values. For $\kappa_n \gg 1$, the large-distance behavior of n/p and $N_\bullet/N_t$ is practically the same.

Finally, we return to justification of our approximation based on the smallness of the ratio $L_D^2/\tilde{R}_D^2$. The values of $\tilde{R}_D = (\varepsilon k_B T/4\pi N_t e^2)^{1/2}$ in undoped materials are typically of the order of 10^2 nm. The diffusion length can be represented as $L_D = (\mu\tau\, k_B T/e)^{1/2}$. The values of $\mu\tau$ can be deduced from measurements of the photoconductivity and/or the photorefractive response in the visible range. The estimate $\mu\tau = 10^{-11}$ cm^2/V is valid for many materials including $BaTiO_3$ [30,31]. With this estimate, we have $L_D \approx 5$ nm. Thus, the ratio $L_D^2/\tilde{R}_D^2$ is very small. Most probably, the condition $L_D^2/\tilde{R}_D^2 \ll 1$ is fulfilled for majority of wide-band-gap ferroelectrics validating the approximation made.

In such a way, not very far from the CDW center, when $e\varphi/k_B T \gtrsim 1$, $n \gg p$, and $N_\bullet = N_t$, the balance equations give the same results as the quasi-Fermi-energy method. For larger distances from the center, when $P(z)$ is already close to $\pm P_0$, the quasi-Fermi-energy method fails. The spatial behavior of P, φ, and n in this far-tail area depends on relationship between different recombination and transport parameters. Under certain simplifying assumptions, it can be described by the balance equations leading to model-dependent far tails of CDWs.

VII. DISCUSSION

Employing systematically the concept of quasi-Fermi energies, we have succeeded in a fairly general, simple, and compact description of the effect of super-band-gap illumination on the CDW properties. The use of the balance equations for electrons and holes has allowed us to extend the range of applicability of the results obtained and to validate them additionally.

Parameter $\kappa_n = \pi P_0^2/2\varepsilon k_B T N_n$, incorporating the basic ferroelectric properties, controls the degree of degeneracy of the compensating electrons near the positive CDWs regardless of illumination. For the negative CDWs, the situation is

analogous: κ_n is trivially replaced by κ_p. For $\kappa_{n,p} \gg 1$, the strongly degenerate carriers form a short-range core of the distribution of the electric potential $\varphi(z)$ [see also Fig. 1(b)]. This core, together with the whole polarization profile $P(z)$, is practically unaffected by light. To the best of our knowledge, this simple and general control was not known earlier.

The super-band-gap illumination substantially decreases the span of the long-range tails of $\varphi(z)$ and slightly reduces their lengths as compared to the case of thermal equilibrium. In other words, light shifts the cores towards CB and VB for the positive and negative CDWs, respectively [see Fig. 1(b)]. For $\kappa \ll 1$, when the compensating free carriers are nondegenerate and the separation in core and tails is not pronounced, light substantially decreases the span of the distributions of $\varphi(z)$ and slightly reduces their widths.

The question arises as to how it is possible to combine a strong charge compensation of the same total polarization charge $2P_0$ with strong variations of the span of the potential profile $\varphi(z)$? The answer is rooted in the general long-range character of the 1D electrostatic screening. Imagine that we have a certain even initial 1D distribution of positive (at the center) and negative (screening) charges, such that the total charge is zero, $\varphi(0)$ is a finite quantity, and $\varphi(\pm\infty) = 0$. Let us now make a spatial redistribution of the screening charge, such that its relatively small fraction is transferred symmetrically over a relatively large distance. In accordance with electrostatics, this redistribution results in arbitrary strong increase of $\varphi(0)$. The effect on $\varphi(0)$ is thus determined by the distance-to-redistributed charge ratio. Strong variations of $\varphi(0)$ for CDWs are fully consistent with the basics.

The substantial light-induced decrease of $\varphi(0)$ has important consequences. First, it decreases substantially the CDW energies. In turn, this facilitates the CDW production within the frustrated poling technique under super-band-gap illumination [13]. We claim that a strong reduction of the CDW energies can contribute to the detected experimental regularities together with the known effect of light heating. Second, one can expect that reduction of $\varphi(0)$ strongly affects the access to the metalliclike conductivity of CDWs. The point is that the potential profile $\varphi(z)$ across the wall must change to a flat profile at the metal electrode. This causes potential barriers [7]. The smaller the variation range of φ across the wall, the easier has to be the contact-barrier problem.

Within our approach, the ratios $r_n = n_0/N_n$ and $r_p = p_0/N_p$ are measures of the illumination strength. For sufficiently small intensity of the super-band-gap illumination I, the linear recombination is dominating and the dependences $n_0, p_0 \propto I$ are expected. With increasing I, the quadratic recombination can become important so that $n_0, p_0 \propto I^{1/2}$. Since the light-absorption coefficient grows rapidly with the light frequency above the band gap and changes from material to material, it is difficult to make reliable estimates of the changeover intensity. However, it can be deduced from the photoconductivity measurements in single-domain crystals [30,31].

Consider lastly what happens when the super-band-gap illumination is switched off. The strong trap saturation $n \gg N_t$ prevents an immediate recombination of electrons unless they are not very far from the core $e\varphi(z)/T \lesssim 1$. This means that the far-tail electrons, such that $e\varphi(z)/k_BT \sim 1$, must diffuse first outwards the wall in order to recombine. However, this out diffusion leads to lowering of the core because of the above-mentioned electrostatic behavior. Ultimately, the top of the core reaches the Fermi level, and the tail experiences a broadening.

VIII. CONCLUSIONS

In conclusion, using the quasi-Fermi-level approach we have investigated the effects of weak super-band-gap illumination on the properties of CDWs in ferroelectrics. Both polarization screening regimes, relevant to degenerate and nondegenerate electrons (holes), are considered. The main impact of light is (i) in a substantial decrease of the span of the electrostatic potential profile $\varphi(z)$ and (ii) in a substantial decrease of the energies of the positively and negatively charged walls as compared to the case of thermal equilibrium. These features have to be important for engineering of CDWs and for the access to the metallic-type wall conductivity. Employment of balance equations for electrons and holes justifies and extends the primary analysis.

ACKNOWLEDGMENT

Financial support from the Presidium Program No. 1 of RAS is acknowledged.

[1] J. Seidel, L. W. Martin, Q. He, Q. Zhan, Y.-H. Chu, A. Rother, M. E. Hawkridge, P. Maksymovych, P. Yu, M. Gajek, N. Balke, S. V. Kalinin, S. Gemming, F. Wang, G. Catalan, J. F. Scott, N. A. Spaldin, J. Orenstein, and R. Ramesh, Conduction at domain walls in oxide multiferroics, Nat. Mater. **8**, 229 (2009).

[2] J. Seidel, P. Maksymovych, Y. Batra, A. Katan, S.-Y. Yang, Q. He, A. P. Baddorf, S. V. Kalinin, C.-H. Yang, J.-C. Yang, Y.-H. Chu, E. K. H. Salje, H. Wormeester, M. Salmeron, and R. Ramesh, Domain Wall Conductivity in La-Doped $BiFeO_3$, Phys. Rev. Lett. **105**, 197603 (2010).

[3] T. Sluka, A. K. Tagantsev, D. Damjanovic, M. Gureev, and N. Setter, Enhanced electromechanical response of ferroelectrics due to charged domain walls, Nat. Commun. **3**, 748 (2012).

[4] M. Schröder, A. Haussmann, A. Thiessen, E. Soergel, T. Woike, and L. M. Eng, Conducting domain walls in lithium niobate single crystals, Adv. Funct. Mater. **22**, 3936 (2012).

[5] D. Meier, J. Seidel, A. Cano, K. Delaney, Y. Kumagai, M. Mostovoy, N. A. Spaldin, R. Ramesh, and M. Fiebig, Anisotropic conductance at improper ferroelectric domain walls, Nat. Mater. **11**, 284 (2012).

[6] P. Maksymovych, A. N. Morozovska, P. Yu, E. A. Eliseev, Y.-H. Chu, R. Ramesh, A. P. Baddorf, and S. V. Kalinin, Tunable metallic conductance in ferroelectric nanodomains, Nano Lett. **12**, 209 (2012).

[7] T. Sluka, A. K. Tagantsev, P. Bednyakov, and N. Setter, Free-electron gas at charged domain walls in insulating $BaTiO_3$, Nat. Commun. **4**, 1808 (2013).

[8] P. Gao, J. Britson, J. R. Jokisaari, C. T. Nelson, S. H. E. Baek, Y. Wang, C. B. Eom, L. Q. Chen, and X. Pan, Atomic-scale mechanisms of ferroelastic domain-wall-mediated ferroelectric switching, Nat. Commun. **4**, 2791 (2013).

[9] R. K. Vasudevan, W. Wu, J. R. Guest, A. P. Baddorf, A. N. Morozovska, E. A. Eliseev, N. Balke, V. Nagarajan, P. Maksymovych, and S. V. Kalinin, Domain wall conduction and polarization-mediated transport in ferroelectrics, Adv. Funct. Mater. **23**, 2592 (2013).

[10] Y. L. Tang, Y. L. Zhu, Y. J. Wang, W. Y. Wang, Y. B. Xu, W. J. Ren, Z. D. Zhang, and X. L. Ma, Atomic-scale mapping of dipole frustration at 90° charged domain walls in ferroelectric $PbTiO_3$ films, Sci. Rep. **4**, 4115 (2014).

[11] P. S. Bednyakov, T. Sluka, A. K. Tagantsev, D. Damjanovic, and N. Setter, Formation of charged ferroelectric domain walls with controlled periodicity, Sci. Rep. **5**, 15819 (2015).

[12] A. Crassous, T. Sluka, A. Tagantsev, and N. Setter, Polarization charge as a reconfigurable quasi-dopant in ferroelectric thin films, Nat. Nanotechnol. **10**, 614 (2015).

[13] P. Bednyakov, T. Sluka, A. Tagantsev, D. Damjanovic, and N. Setter, Free-carrier-compensated charged domain walls produced with super-bandgap illumination in insulating ferroelectrics, Adv. Mater. **28**, 9498 (2016).

[14] L. Li, J. Britson, J. R. Jokisaari, Y. Zhang, C. Adamo, A. Melville, D. G. Schlom, L. Chen, and X. Pan, Giant resistive switching via control of ferroelectric charged domain walls, Adv. Mater. **28**, 6574 (2016).

[15] T. Sluka, P. Bednyakov, P. Yudin, A. Crassous, and A. Tagantsev, Charged domain walls in ferroelectrics, in Topological Structures in Ferroic Materials, Springer Ser. Mater. Sci. **228**, 103 (2016).

[16] S. Y. Yang, J. Seidel, S. J. Byrnes, P. Shafer, C.-H. Yang, M. D. Rossell, P. Yu, Y.-H. Chu, J. F. Scott, J. W. Ager, L. W. Martin, and R. Ramesh, Above-band gap voltages from ferroelectric photovoltaic devices, Nat. Technol., **5**, 143 (2010).

[17] J. Seidel, D. Fu, S.-Y. Yang, E. Alarcón-Lladó, J. Wu, R. Ramesh, and J. W. Ager, Efficient Photovoltaic Current Generation at Ferroelectric Domain Walls, Phys. Rev. Lett. **107**, 126805 (2011).

[18] J. E. Spanier, V. M. Fridkin, A. M. Rappe, A. R. Akbashev, A. Polemi, Y. Qi, Z. Gu, S. M. Young, C. J. Hawley, D. Imbrenda, G. Xiao, A. L. Bennett-Jackson, and C. L. Johnson, Power conversion efficiency exceeding the Shockley-Queisser limit in a ferroelectric insulator, Nat. Photonics **10**, 611 (2016).

[19] G. Catalan, J. Seidel, R. Ramesh, and J. F. Scott, Domain wall nanoelectronics, Rev. Mod. Phys. **84**, 119 (2012).

[20] B. M. Vul, G. M. Guro, and I. Ivanchik, Encountering domains in ferroelectrics, Ferroelectrics **6**, 29 (1973).

[21] I. I. Ivanchik, Spontaneous polarization screening in a single domain ferroelectric, Ferroelectrics **145**, 149 (1993).

[22] M. Y. Gureev, A. K. Tagantsev, and N. Setter, Head-to-head and tail-to-tail 180° domain walls in an isolated ferroelectric, Phys. Rev. B **83**, 184104 (2011).

[23] E. A. Eliseev, A. N. Morozovska, G. S. Svechnikov, V. Gopalan, and V. Y. Shur, Static conductivity of charged domain walls in uniaxial ferroelectric semiconductors, Phys. Rev. B **83**, 235313 (2011).

[24] Z. Li, H. Wu, and W. Cao, Piezoelectric response of charged non-180° domain walls in ferroelectric ceramics, J. Appl. Phys. **111**, 024106 (2012).

[25] M. Y. Gureev, P. Mokrý, A. K. Tagantsev, and N. Setter, Ferroelectric charged domain walls in an applied electric field, Phys. Rev. B **86**, 104104 (2012).

[26] P. Ondrejkovic, P. Marton, M. Guennou, N. Setter, and J. Hlinka, Piezoelectric properties of twinned ferroelectric perovskites with head-to-head and tail-to-tail domain walls, Phys. Rev. B **88**, 024114 (2013).

[27] Y. Zuo, Yu. A. Genenko, and B.-X. Xu, Charge compensation of head-to-head and tail-to-tail domain walls in barium titanate and its influence on conductivity, J. Appl. Phys. **116**, 044109 (2014).

[28] P. V. Yudin, M. Y. Gureev, T. Sluka, A. K. Tagantsev, and N. Setter, Anomalously thick domain walls in ferroelectrics, Phys. Rev. B **91**, 060102(R) (2015).

[29] B. Sturman, E. Podivilov, M. Stepanov, A. Tagantsev, and N. Setter, Quantum properties of charged ferroelectric domain walls, Phys. Rev. B **92**, 214112 (2015).

[30] *Photorefractive Materials and Their Applications I, Fundamental Phenomena*, edited by P. Günter and J.-P. Huignard (Springer, Berlin, 1988), Vol. 61.

[31] *Photorefractive Materials and Their Applications, Basic Effects*, edited by P. Günter and J.-P. Huignard (Springer, Berlin, 2007).

[32] S. M. Sze, *Semiconductor Devices Physics and Technology* (Wiley, New York, 1985).

[33] K. Seeger, *Semiconductor Physics* (Springer, Berlin, 1973).

[34] P. Bernasconi, G. Montemezzani, I. Biaggio, and P. Günter, Characterization of the bipolar mobility in polar materials by interband photoexcitation, Phys. Rev. B **56**, 12196 (1997).

[35] V. L. Bonch-Bruevich and S. G. Kalashnikov, *Physics of Semiconductors* (Nauka, Moscow, 1977), p. 208.

[36] D. K. Ferry, *Semiconductors, Bonds and Bands* (IOP Publishing, Bristol, UK, 2013).